THE JOURNAL OF PHYSICAL CHEMISTRY C

ARTICLE

pubs.acs.org/JPCC

Microstructure and Phase Behavior of a Quinquethiophene-Based Self-Assembled Monolayer as a Function of Temperature

Heinz-Georg Flesch,[†] Simon G. J. Mathijssen,[‡,§] Fatemeh Gholamrezaie,[‡,∥] Armin Moser,[†] Alfred Neuhold,[†] Jirí Novák,[†] Sergei A. Ponomarenko,[⊥] Quan Shen,[#] Christian Teichert,[#] Gregor Hlawacek,[#,▽] Peter Puschnig,[○] Claudia Ambrosch-Draxl,[○] Roland Resel,[*,†] and Dago M. de Leeuw[‡,∥]

[†]Institute of Solid State Physics, Graz University of Technology, Petersgasse 16, 8010 Graz, Austria

[‡]Philips Research Laboratories, High Tech Campus 4, 5656 AE Eindhoven, The Netherlands

[§]Department of Applied Physics, Eindhoven University of Technology, P.O. Box 513, 5600 MB Eindhoven, The Netherlands

[∥]Molecular Electronics, Zernike Institute for Advanced Materials, University of Groningen, Nijenborgh 4, 9747 AG Groningen, The Netherlands

[⊥]Enikolopov Institute of Synthetic Polymeric Materials of the Russian Academy of Sciences, Profsoyuznaya 70, 117393 Moscow, Russia

[#]Institute of Physics and [○]Chair of Atomistic Modeling and Design of Materials, Montanuniversitaet Leoben, Franz-Josef-Straße 18, 8700 Leoben, Austria

[▽]Physics of Interfaces and Nanomaterials, MESA+ Institute for Nanotechnology, University of Twente, P.O. Box 217, 7500 AE Enschede, The Netherlands

ABSTRACT: The self-assembly of monolayers is a highly promising approach in organic electronics, but most systems show weak device performances, probably because of a lack of long-range order of the molecules. The present self-assembled monolayer was formed by a molecule that contains a dimethylchlorosilyl group combined with a quinquethiophene unit through an undecane spacer. This system is the first reported self-assembled monolayer on silicon oxide surfaces that forms two-dimensional crystals. A detailed structural solution is presented based on grazing-incidence X-ray scattering experiments and theoretical packing analysis. By transverse shear microscopy, the shape and size of the crystallites were determined: polygonal shapes with lateral sizes of several micrometers were observed. In situ temperature studies revealed gradual changes of the molecular packing that were irreversible. Melting of the crystal structure was found at 520 K, whereas the self-assembled monolayer remained stable up to 620 K. This work presents unknown structural properties of a self-assembled monolayer revealing insights into layer formation and irreversible evolution upon temperature treatment.

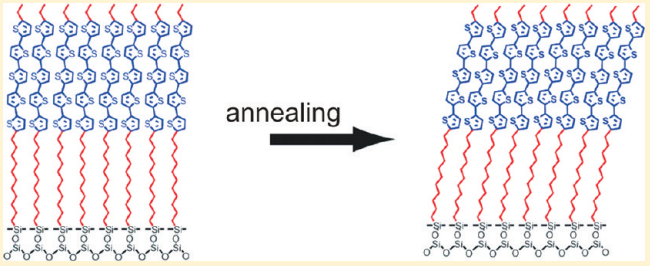

INTRODUCTION

Self-assembly of monolayers represents a key technology in organic electronics. An established technique, known since the 1980s, is monolayer formation from solution on silicon dioxide.[1] The field of self-assembled monolayers (SAMs) in general[2,3] and of SAMs on silicon dioxide[4−6] in particular has been reviewed several times. It has been demonstrated that transport in organic field-effect transistors is determined by the first monolayer of the organic semiconductor and its interface properties.[7,8] The width of the accumulation layer is at most a few nanometers, and the charge transport occurs solely at the gate dielectric−semiconductor interface.[9−11] Therefore, the concept of SAMs as semiconductors in field-effect transistors (FETs) has attracted much attention in the field of organic electronics, as SAMFETs could be used as basic building blocks of self-assembled electronics.[12,13] A quinquethiophene-based SAMFET was recently reported, and it was shown that its key device parameters were identical to those of bulk thin-film transistors.[12,14] The molecule (inset of Figure 1b) has a dimethylchlorosilane anchoring group that can be grafted onto a hydroxylated silicon dioxide substrate.[15] An undecane spacer is incorporated to provide flexibility for the arrangement of the semiconducting quinquethiophene backbone. The molecule is end-capped with an ethyl group. It is well-known that, for efficient charge transport, a highly ordered system with overlapping π orbitals is required,[16] as demonstrated, for example, for pentacene monolayers[7] and oligothiophenes.[17]

In this work, we determined the morphology and crystallographic packing as a function of temperature for the first reported crystalline SAM on silicon dioxide. This is an important step toward technological realization of SAM-based electronics as practical applications of such devices require a large temperature budget. We found that two-dimensional crystals are generated

Received: June 27, 2011
Revised: October 11, 2011
Published: October 18, 2011

dx.doi.org/10.1021/jp206033x | J. Phys. Chem. C 2011, 115, 22925–22930

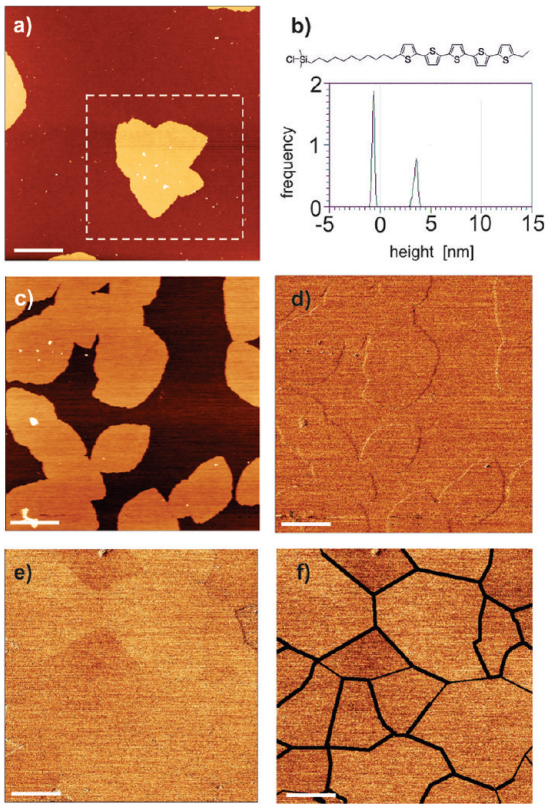

Figure 1. (a) Atomic force microscopy topography image (recorded in tapping mode) of a pristine submonolayer SAM showing a polygonal shaped island. (b) Height histogram of the area shown in panel a, revealing an island average height of 42 Å. (c) Topography image (recorded in contact mode) of a pristine submonolayer SAM and (d) corresponding TSM image showing no shear force contrast (apart from morphology-induced artifacts at the islands' edges). (e) TSM image of a SAM annealed at 400 K. (f) Image e with additionally drawn clear domain boundaries (thick lines) and proposed boundaries (thin lines). The scale bars correspond to 6 μm.

during layer formation and that a gradual crystalline phase transition occurs upon temperature treatment.

EXPERIMENTAL METHODS

Sample Preparation. Monolayer preparation using chloro [11-(5‴″-ethyl-2,2′:5′,2″:5″,2‴:5‴,2⁗:5⁗,2⁗′-quinquethien-5-yl)undecyl]-dimethylsilane on {001} cut Si wafers with 205-nm thermal dioxide has been described previously.[12,14] To obtain full coverage, the substrate was immersed for one day in a solution of dissolved active molecules. Lower immersion times resulted in submonolayer coverages of the substrate, whereas longer immersion times did not result in the formation of multilayers. Samples with both submonolayer and full monolayer coverages were investigated in their pristine state (i.e., directly after being removed from solution) and additionally after 400 K temperature treatment in a vacuum for 1 h, as was done for the reported SAMFETs.

X-ray Diffraction Techniques. X-ray scattering experiments were performed under grazing-incidence conditions at the ID10B at the European Synchrotron Radiation Facility (ESRF) in Grenoble, France.[18] In situ temperature studies were performed using a domed heating stage DHS900[19] from Anton Paar Ltd. with a PEEK dome providing a protective He atmosphere for grazing-incidence X-ray diffraction (GIXD) experiments. Samples were mounted horizontally and tilted with respect to the incident beam to adjust the angle of incidence. For signal detection in all GIXD experiments, we used a gas-filled position-sensitive wire detector. Reciprocal-space data are presented.

X-ray reflectivity (XRR) measurements were performed on a Bruker D8 Discover diffractometer using Cu K_α radiation. The primary optics were set by a parallelizing Goebel mirror. A DHS1100 domed heating stage provided by Anton Paar Ltd. with a PEEK dome and He atmosphere for sample protection was used. Simulations of the XRR data were based on a two-layer model for the SAM layer with two different mean electron densities (see an earlier work on the same system[12]). One layer represented the alkyl spacer groups, and the second represented the top layer of the thiophene backbones. Calculation of the parameters was performed using Parratt's recursive algorithm,[20] and the influence of roughness was taken into account by the approach proposed by Nevot and Croce.[21] The evaluation was implemented in WinGixa simulation software.[22] The total layer thickness was always found to be above the theoretically expected value of 36 Å.

Atomic Force Microscopy (AFM). Measurements were performed on an Asylum Research MFP 3D stand-alone atomic force microscope using PPP-LFMR (PointProbe Plus Lateral Force Microscopy) probes from NanoSensors. The probes have a typical force constant of 0.2 N m^{-1} and a guaranteed tip radius of less than 10 nm. The scans were performed with forces between 1.1 nN and 5.5 nN. Transverse shear microscopy (TSM)[23,24] was employed to investigate the morphology, shape, and crystallographic orientation of grains in the layers. In TSM, the probe is scanned in contact mode parallel to the cantilever's long axis. The torsion of the cantilever induced by the different crystallographic alignment of tilted molecules can be recorded by the four-quadrant photodiode. An isotropic surface, such as one formed from molecules standing exactly upright, will yield no contrast in TSM mode. The information obtained by TSM is supported by topographic images. To determine the height of submonolayer islands, topographic images in tapping mode were also recorded using PPP-NCHR (Non-Contact/High Resonance Frequency) probes from NanoSensors (force constant = 10−130 N/m). To avoid any deformation of the SAM, these measurements were performed with the smallest forces possible to still guarantee stable imaging conditions.

Density Functional Theory. Ab initio calculations within the framework of density functional theory (DFT) were used to determine the molecular packing angle of the quinquethiophene units within the SAMs. We utilized the VASP code[25,26] and employed a generalized gradient approximation for exchange and correlation effects,[27] which has proven capable of correctly accounting for the herringbone packing of rodlike molecules.[28] The structural model was based on the two-dimensional unit-cell parameters obtained from the X-ray diffraction experiments assuming a free-standing layer of quinquethiophene molecules in a herringbone arrangement. For these calculations, the alkyl spacer groups were neglected. Note that the asymmetric 5T molecules can be arranged in two different ways within the unit cell. The difference is a 180° rotation of the centered molecule around its long molecular axis. This does not affect the position of the energetic minimum. Hence, it can be assumed that the film shows both types of neighboring molecular orientations.

Table 1. Unit-Cell Parameters (a, b, γ), Molecular Packing Parameters (Tilt Angle θ, Tilt Direction Ω, Herringbone Angle β), and Unit-Cell Volume Given for the Phase of Upright-Standing Molecules (Pristine) and the Phase of Tilted Molecules (Annealed at 400 K)

state	a (Å)	b (Å)	γ (deg)	tilt angle θ (deg)	tilt direction Ω (deg)	packing angle β (deg)	volume (Å^{-3})
pristine state	5.6 ± 0.2	7.2 ± 0.2	90 ± 2	0	–	63	456 ± 7
annealed at 400 K	5.6 ± 0.2	8.1 ± 0.2	90 ± 2	13 ± 2	0 ± 3	60	462 ± 11

RESULTS AND DISCUSSION

Pristine Layers. The structure of the SAM in the pristine state, that is, after removal of the sample from solution without temperature treatment, shows a homogeneous, smooth, and densely packed monolayer of molecules standing fully upright with unit-cell parameters of a = 5.6 Å, b = 7.2 Å, and γ = 90° (Table 1). These values are comparable to those reported previously for the same system.[12,14] Formation of the crystalline structure does not yield a unique unit cell; the variation of the unit-cell parameters is reported in Table 1. Neither a correlation between the immersion time in solution and the size of the unit cell nor a tendency for the size of the unit cell to change from the submonolayer to the closed monolayer state was found. Although the size of the unit cell varied [average volume per molecule = (456 ± 7) Å^3], the packing of the molecules demonstrated a herringbone motif, as generally found in oligothiophenes.[29] Because the alkyl spacer groups do not provide a detectable structural scattering signal, it was not possible to judge their ordering, although long-range order has already been detected in alkyl-based SAMs.[30]

Figure 1a shows the morphology of a film with submonolayer coverage recorded in tapping mode. It shows polygonal-shaped islands with a lateral size in the range of 10 μm. The corresponding height histogram reveals an average island height of 42 Å, which is close to the length of the stretched molecule (36 Å). The submonolayer was built from molecules standing exactly upright, as confirmed by the appearance of Bragg rods with maxima at the Yoneda horizon[31] (q_z = 0.025 Å^{-1}) and a smoothly decreasing intensity toward higher q_z observed by GIXD (Figure 2a). Consequently, no contrast between individual domains was obtained by TSM, as can be seen from the shear force contrast image presented in Figure 1d. Figure 1c presents the simultaneously recorded topography image.

Layers Annealed at 400 K. Heat-treated samples were investigated by AFM, which showed smooth layers. Crystalline domains with rims of approximately 0.5 Å height at the grain boundaries were found. TSM images (Figure 1e) show polygonal domains of different contrast (similar in shape and size to the islands in the submonolayer in Figure 1a,c). This contrast is the result of different azimuthal orientations of the tilted quinquethiophene units of the molecule. Panels e and f of Figure 1 show the same image but with the domain boundaries emphasized by black lines, as guides for the eye, in Figure 1f. The thin lines represent domain boundaries that were inserted based on additional TSM and topography images recorded with different forces, providing different contrasts.

GIXD was employed to verify the molecular tilt found by TSM and to evaluate its magnitude. Figure 2b shows an indexed reciprocal-space map of a SAM annealed at 400 K. An area of increased intensity of the Bragg rod was found above the Yoneda horizon[31] (q_z = 0.025 Å^{-1}), indicating that, upon annealing, a transition from a phase with upright-standing molecules (Bragg rods, Figure 2a) to a phase of tilted molecules occurred.[32] Even within one sample, the tilt of the molecules, and hence the size of the unit cell varied slightly, causing the Bragg rods to have an arclike shape in GIXD.

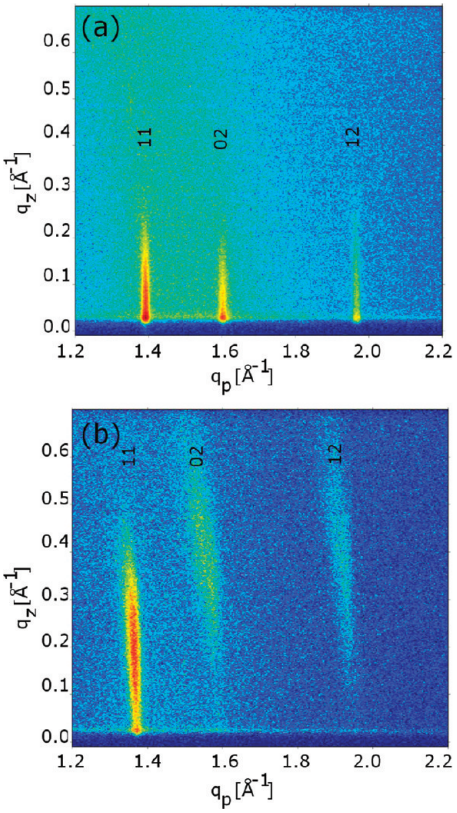

Figure 2. Reciprocal-space maps of (a) a pristine SAM of upright-standing molecules and (b) a SAM annealed at 400 K showing the footprint of tilted molecules.

The difference in the reciprocal-space map between the SAMs annealed at 400 K and the pristine layers[12,14] is emphasized by the line cuts along q_z given for the 11, 02, and 12 rods in Figure 3. The maximum of the 11 Bragg rod of the phase of tilted molecules occurred at q_p = 1.36 Å^{-1} and q_z = 0.2 Å^{-1}, that of the 02 reflection at q_p = 1.55 Å^{-1} and q_z = 0.39 Å^{-1}, and that of the 12 reflection at q_p = 1.91 Å^{-1} and q_z =0.44 Å^{-1}. From these data, unit-cell parameters were calculated (Table 1) using a theory established in refs 32−34. The unit cell remained rectangular, as found for the pristine phase. From the q_z positions of the peak maxima along the Bragg rods, a tilt of the molecules of θ = (13 ± 2)° was calculated. For the direction of the tilt, we define Ω as the azimuthal angle between the projection of the long molecular axis onto the ab plane and the b axis (compare Figure 4a). Within the experimental precision, this angle was found to be 0° for all samples. Hence, only the unit-cell parameter b increased when the molecules tilted.

The width of the Bragg rod in the q_z direction was determined from the length (L) of the molecule, as given by $2\pi L^{-1}$.[28]

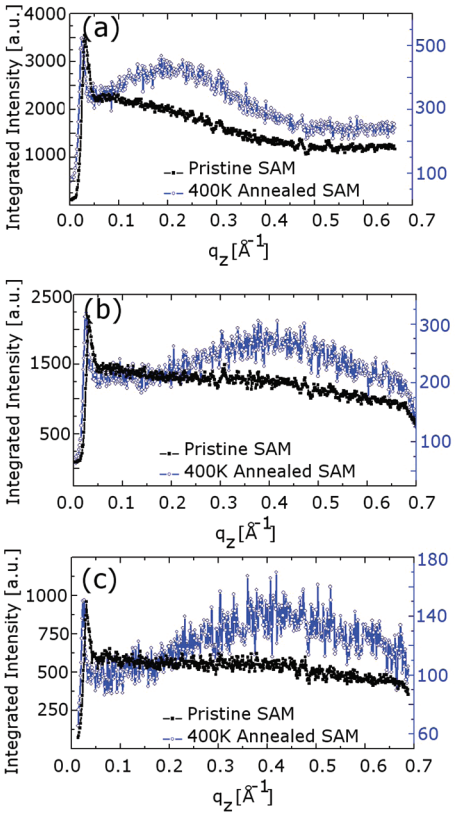

Figure 3. Intensity integrated along q_p for (a) the 11 Bragg rod, (b) the 02 Bragg rod, and (c) the 12 Bragg rods for the pristine SAM (left scale) and the SAM annealed at 400 K (right scale) from the reciprocal-space maps of Figure 2.

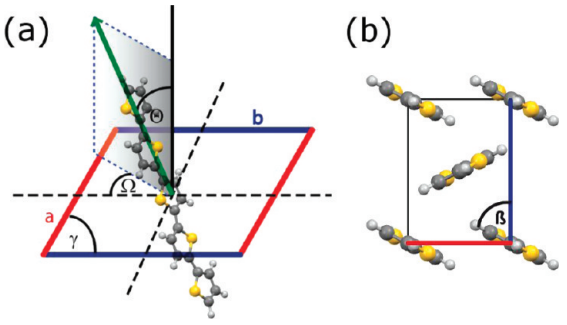

Figure 4. (a) Schematic view of the orientation of an individual molecule (tilt angle θ, tilt azimuth Ω) within the two-dimensional unit cell (a, b, γ). (b) View along the long molecular axes giving the location of the herringbone angle β.

From the full width at half-maximum (q_z), we calculated a length of 21 Å, which is in excellent agreement with the length of the quinquethiophene backbone. The amorphous alkyl spacer does not contribute to the Bragg rods and can be neglected in the considerations of the crystalline layer.

Packing of the Molecules. From the dominant reflections (11, 02, and 12), a herringbone packing was deduced. DFT calculations were employed to clarify the molecular arrangement for both phases because this information is not accessible from the experimental data. Unit-cell parameters a, b, and γ and the tilt of the molecules θ (0°, 13°) were used as input for the geometry

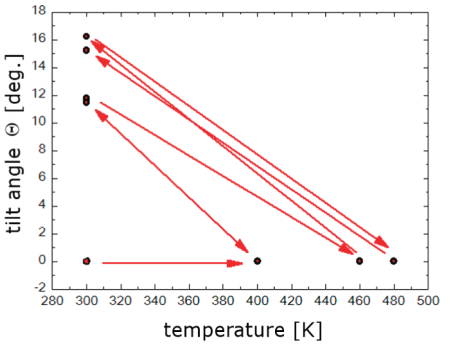

Figure 5. Evolution of the molecular tilt angle θ during in situ temperature cycling of the sample. Arrows indicate the chronology of the experiment.

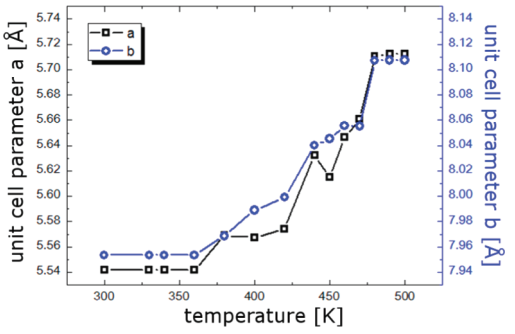

Figure 6. Evolution of the unit-cell parameters a (left scale) and b (right scale) as a function of temperature of a SAM pretreated by annealing at 400 K.

relaxations. The DFT-optimized herringbone angles were found to be β = 63° for the pristine layers and β = 60° for the SAMs annealed at 400 K, where we define β as the angle between the aromatic plane of the molecule and the b lattice vector (Figure 4b).

In Situ Temperature Studies. Investigations on the thermal stability of the microstructure were performed in situ by GIXD and XRR. GIXD investigations gave the tilt angle of the molecules as a function of temperature (Figure 5). The in situ studies revealed that the quinquethiophene units were always standing upright at elevated temperatures (θ = 0°). However, after thermal treatment, distinct tilt angles were observed at room temperature (T = 300 K). The tilt angle increased with the temperature of heat treatment to a value of 17°. These changes in the molecular tilt angle were irreversible. Similar temperature-induced changes of the tilt angle have been observed in SAMs of phosphonic acids.[35]

The unit-cell parameters as a function of temperature (Figure 6) show that the enlargement of the unit cell was isotropic. The lattice constants expanded by about 0.2 Å in the temperature range from 300 to 500 K. The observed thermal expansion is comparable to that of other SAMs on silicon oxide surfaces.[36] The crystalline structure was lost at 520 K, in excellent agreement with the melting temperature of 526 K reported for quinquethiophene.[37] Several heating and cooling steps in the range between 300 and 520 K showed that the crystalline order could not be improved or recovered by temperature; hence, we conclude the crystalline order is induced during the formation of the layer and, therefore, depends strongly on the preparation of the substrate.

The thermal expansion of the unit cell was not fully reversible, so that a slightly expanded lattice remained after the heat treatment.

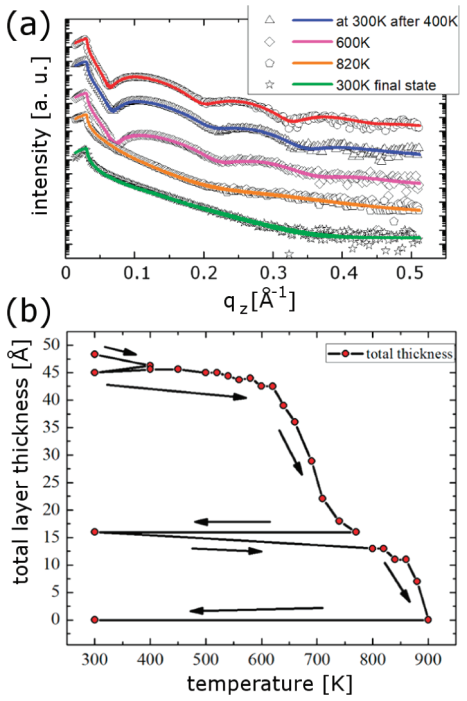

Figure 7. (a) X-ray reflectivity measurements during the temperature treatment of a SAM. The data (symbols) are presented together with the simulations (lines) from WinGixa. The curves are shifted for clarity. (b) Evolution of the total layer thickness due to heating and cooling of the sample, where the arrows indicate the sequence of the experiment.

Considering the change in the molecular tilt angle together with the irreversible lattice expansion, a volume of the unit cell of (470 ± 13) Å^3 was observed after heat treatment at 500 K (compare Table 1).

The XRR results (Figure 7) revealed a constant layer thickness up to 620 K that was satisfactorily described with a two-layer model assuming two different electron densities for the thiophenes and the alkyl groups. Above 620 K, a single-layer model with an average electron density described the experimental data well, indicating a transition from a layered structure to a disordered layer with a heat-induced decrease in layer thickness. The layer thickness remained stable even when the film was cooled (constant layer thickness of 16 Å upon cooling from 780 to 300 K; Figure 7b). It can be expected that, at elevated temperatures, cracking of the molecules occurds so that the layer partially decomposed.[38] The complete desorption of the SAM were observed above 880 K.

Because temperature treatment did not show any impact on the domain size, it can be concluded that the morphology and size of the crystalline domains of the SAM are determined during layer formation. This is supported by the correspondence in shape between the submonolayer islands and the crystalline domains (Figure 1) and by diffraction experiments in which no healing or recovery effects of the crystalline order by the influence of temperature were observed. Annealing below 520 K always yielded a phase of tilted molecules, in contrast to the upright-standing molecules in the pristine films.

The almost reversible increase of the unit cell during the temperature treatment can be considered a result of thermal expansion, whereas the irreversible expansion of approximately 10% suggests partial desorption of less strongly bound (physisorbed) molecules. This irreversibility within the sample is also reflected in the irreversible increase of the tilt angle of the molecules after temperature treatment.

CONCLUSIONS

Detailed structural and morphological investigations of the two-dimensional crystal structure of a quinquethiophene-based SAM have shown that different phases can be found depending on the sample thermal history. In the pristine state and at elevated temperature, the molecules stand exactly upright on the surface. Upon temperature treatment, the molecules tilt toward the *b* axis of the unit cell, but no impact of temperature on the domain size was found. In situ investigations at temperatures up to 520 K revealed an almost reversible isotropic expansion of the unit cell, and melting of the crystal was observed above 520 K. Between 520 and 620 K, a layered SAM with amorphous quinquethiophene units was present. The layered order was lost above 620 K, and a disordered state formed that desorbed completely at 880 K. The two-dimensional ordering in this SAM is induced by the layer formation process, during which single-crystalline domains with polygonal shapes are formed with a lateral size in the micrometer range. The crystal structure shows a certain variation of both the lattice constants and the molecular packing that is related to the specific nature of self-assembled monolayers formed by partial covalent bonding of the molecules to the substrate.

AUTHOR INFORMATION

Corresponding Author

*Tel.: +43-316-873-8476. Fax: +43-316-873-8466. E-mail: roland.resel@tugraz.at.

ACKNOWLEDGMENT

We acknowledge E. C. P. Smits and H. J. Wondergem for fruitful discussions, the ESRF for providing synchrotron radiation, and Oleg Konovalov for his assistance in using beamline ID10B. Financial support from the Austrian Research Promotion Agency within the project ISOTEC, the Austrian Science Fund (S9707-N20 and S9714), the Dutch Technology Foundation STW, and the EU project ONE-P (no. 212311) is acknowledged. S.A.P. thanks Heraeus Precious Metals for financial support.

REFERENCES

(1) Sagiv, J. *J. Am. Chem. Soc.* **1980**, *102*, 92–98.
(2) Schreiber, F. *Prog. Surf. Sci.* **2000**, *65*, 151–257.
(3) Heimel, G.; Rissner, F.; Zojer, E. *Adv. Mater.* **2010**, *22*, 2494–2513.
(4) Onclin, S.; Ravoo, B. J.; Reinhoudt, D. N. *Angew. Chem., Int. Ed.* **2005**, *44*, 6282–6304.
(5) Wen, K.; Maoz, R.; Cohen, H.; Sagiv, J.; Gibaud, A.; Desert, A.; Ocko, B. M. *ACS Nano* **2008**, *2*, 579–599.
(6) Haensch, C.; Hoeppener, S.; Schubert, U. S. *Chem. Soc. Rev.* **2010**, *39*, 2323–2334.
(7) Mannsfeld, S. C. B.; Virkar, A.; Reese, C.; Toney, M. F.; Bao, Z. *Adv. Mater.* **2009**, *21*, 2294–2298.
(8) Lee, H. S.; Kim, D. H.; Cho, J. H.; Hwang, M.; Jang, Y.; Cho, K. *J. Am. Chem. Soc.* **2008**, *130*, 10556–10564.
(9) Dinelli, F.; Murgia, M.; Levy, P.; Cavallini, M.; Biscarini, F.; de Leeuw, D. M. *Phys. Rev. Lett.* **2004**, *92*, 116802.
(10) Muck, T.; Fritz, J.; Wagner, V. *Appl. Phys. Lett.* **2005**, *86*, 232101.
(11) Quiroga, S. D.; Shehu, A.; Albonetti, C.; Murgia, M.; Stoliar, P.; Borgatti, F.; Biscarini, F. *Rev. Sci. Instrum.* **2011**, *82*, 025110.

(12) Smits, E. C. P.; Mathijssen, S. G. J.; van Hal, P. A.; Setayesh, S.; Geuns, T. C. T.; Mutsaers, K. A. H. A.; Cantatore, E.; Wondergem, H. J.; Werzer, O.; Resel, R.; Kemerink, M.; Kirchmeyer, S.; Muzafarov, A. M.; Ponomarenko, S. A.; de Boer, B.; Blom, P. W. M.; de Leeuw, D. M. *Nature* **2008**, *455*, 956–959.
(13) Novak, M.; Ebel, A.; Meyer-Friedrichsen, T.; Jedaa, A.; Vieweg, B. F.; Yang, G.; Voitchovsky, K.; Stellacci, F.; Spiecker, E.; Hirsch, A.; Halik, M. *Nano Lett.* **2011**, *11*, 156–159.
(14) Mathijssen, S. G. J.; Smits, E. C. P.; van Hal, P. A.; Wondergem, H. J.; Ponomarenko, S. A.; Moser, A.; Resel, R.; Bobbert, P. A.; Kemerink, M.; Janssen, R. A. J.; de Leeuw, D. M. *Nat. Nanotechnol.* **2009**, *4*, 674–680.
(15) Ponomarenko, S. A.; Borshchev, O. V.; Meyer-Friedrichsen, T.; Pleshkova, A. P.; Setayesh, S.; Smits, E. C. P.; Mathijssen, S. G. J.; de Leeuw, D. M.; Kirchmeyer, S.; Muzafarov, A. M. *Organometallics* **2010**, *29*, 4213–4226.
(16) Mottaghi, M.; Horowitz, G. *Org. Electron.* **2006**, *7*, 528–536.
(17) Dholakia, G. R.; Meyyappan, M.; Facchetti, A.; Marks, T. J. *Nano Lett.* **2006**, *6*, 2447–2455.
(18) Smilgies, D.-M.; Boudet, N.; Struth, B.; Konovalov, O. *J. Synchrotron Radiat.* **2005**, *12*, 329–339.
(19) Resel, R.; Tamas, E.; Sonderegger, B.; Hofbauer, P.; Keckes, J. *J. Appl. Crystallogr.* **2003**, *36*, 80–85.
(20) Parratt, L. G. *Phys. Rev.* **1954**, *95*, 359–369.
(21) Névot, L.; Croce, P. *Rev. Phys. Appl.* **1980**, *15*, 761–769.
(22) Leenaers, A. J. G.; de Boer, D. K. G. *X-Ray Spectrom.* **1997**, *26*, 115–121.
(23) Puntambekar, K.; Dong, J.; Haugstad, G.; Frisbie, C. D. *Adv. Funct. Mater.* **2006**, *16*, 879–884.
(24) Zhang, J.; Rabe, J. P.; Koch, N. *Adv. Mater.* **2008**, *20*, 3254–3257.
(25) Kresse, G.; Furthmüller, J. *Phys. Rev. B* **1996**, *54*, 11169–11186.
(26) Kresse, G.; Furthmüller, J. *Comput. Mater. Sci.* **1996**, *6*, 15–50.
(27) Perdew, J. P.; Burke, K.; Ernzerhof, M. *Phys. Rev. Lett.* **1996**, *77*, 3865–3868.
(28) Hummer, K.; Puschnig, P.; Ambrosch-Draxl, C. *Phys. Rev. B* **2003**, *67*, 184105.
(29) Fichou, D. *Handbook of Oligo- and Polythiophenes*; Wiley-VCH: New York, 1999.
(30) Koga, T.; Morita, M.; Ishida, H.; Yakabe, H.; Sasaki, S.; Sakata, O.; Otsuka, H.; Takahara, A. *Langmuir* **2005**, *21*, 905–910.
(31) Yoneda, Y. *Phys. Rev.* **1963**, *131*, 2010–2013.
(32) Kjaer, K. *Physica B: Condens. Matter* **1994**, *198*, 100–109.
(33) Cavalcanti, L.; P. Konovalov, O.; Torriani, I. L. *Eur. Biophys. J.* **2006**, *35*, 431–438.
(34) Wiegart, L.; Struth, B. *Physica B: Condens. Matter* **2005**, *357*, 126–129.
(35) De Pauli, M.; Pérez, C. A.; Prado M. C.; Araújo, D. H. C.; Neves, B. R. A.; Malachias A. Energy dispersive X-ray reflectivity applied to the study of thermal stability of self-assembled organic multilayers: Results on phosphonic acids. *Synth. Met.*, published online Sep 29, 2011, http://dx.doi.org/10.1016/j.synthmet.2011.09.010.
(36) Tidswell, I. M.; Rabedeau, T. A.; Pershan, P. S.; Kosowsky, S. D.; Folkers, J. P.; Whitesides, G. M. *J. Chem. Phys.* **1991**, *95*, 2854–2861.
(37) Wolfer, P.; Müller, C.; Smith, P.; Baklar, M. A.; Stingelin-Stutzmann, N. *Synth. Met.* **2007**, *157*, 827–833.
(38) Kluth, G. J.; Sung, M. M.; Maboudian, R. *Langmuir* **1997**, *13*, 3775–3780.